DNA damage and genome instability by G-quadruplex ligands are mediated by R loops in human cancer cells

Alessio De Magis[a,1,2], Stefano G. Manzo[a,1,3], Marco Russo[a], Jessica Marinello[a], Rita Morigi[a], Olivier Sordet[b], and Giovanni Capranico[a,4]

[a]Department of Pharmacy and Biotechnology, Alma Mater Studiorum University of Bologna, 40126 Bologna, Italy; and [b]Cancer Research Center of Toulouse, INSERM, Université de Toulouse, Université Toulouse III Paul Sabatier, CNRS, 31037 Toulouse, France

Edited by Philip C. Hanawalt, Stanford University, Stanford, CA, and approved December 3, 2018 (received for review June 16, 2018)

G quadruplexes (G4s) and R loops are noncanonical DNA structures that can regulate basic nuclear processes and trigger DNA damage, genome instability, and cell killing. By different technical approaches, we here establish that specific G4 ligands stabilize G4s and simultaneously increase R-loop levels within minutes in human cancer cells. Genome-wide mapping of R loops showed that the studied G4 ligands likely cause the spreading of R loops to adjacent regions containing G4 structures, preferentially at 3′-end regions of expressed genes, which are partially ligand-specific. Overexpression of an exogenous human RNaseH1 rescued DNA damage induced by G4 ligands in *BRCA2*-proficient and *BRCA2*-silenced cancer cells. Moreover, even if the studied G4 ligands increased noncanonical DNA structures at similar levels in nuclear chromatin, their cellular effects were different in relation to cell-killing activity and stimulation of micronuclei, a hallmark of genome instability. Our findings therefore establish that G4 ligands can induce DNA damage by an R loop-dependent mechanism that can eventually lead to different cellular consequences depending on the chemical nature of the ligands.

R loop | G-quadruplex ligand | genome instability | DNA cleavage | antitumor activity

G quadruplexes (G4s) are noncanonical secondary DNA structures constituted of two or more stacked guanine tetrads held together by Hoogsteen hydrogen bonds and stabilized by monovalent cations such as K^+ and Na^+ (1, 2). G4s can play a regulatory role in basic nuclear functions such as replication and transcription, and indeed G4-promoting sequences have been mapped at key regulatory genomic sites, notably oncogene promoters, untranslated exonic regions, replication origins, and telomeres (1, 2). In the past years, several specific G4 ligands have been developed targeting telomeres or oncogene promoters, as G4s are considered promising targets of effective anticancer drugs (1, 2). Nevertheless, despite the high number of G4 ligands in the literature, few have entered early phases of clinical trials and none has shown efficacy in cancer patients (1–3).

An intriguing effect of G4 ligands is the induction of DNA damage and genome instability. In particular, pyridostatin (PDS) (*SI Appendix*, Fig. S1*A*), a well-known G4 ligand (1, 4), induces DNA damage as shown by formation of γH2AX foci (5), a marker of double-stranded DNA breakage (DSB). The compound triggers the activation of the DNA damage response (DDR) pathway, as determined by phosphorylation of ATM, DNA-PKcs, Chk1, and other factors and by cell-cycle arrest at G2/M phase (5). G4 ligands, including PDS, were recently shown to be more active in reducing the proliferation of *BRCA1/2*-deficient cancer cells by accumulating DNA damage, chromosomal aberrations, and persistent checkpoint activation (6, 7). These findings are consistent with a critical role of the homologous recombination repair (HRR) pathway in protecting cancer cells from genome instability triggered by G4 ligand activity. Consistently, G4 structures can lead to instability of the CEB1 minisatellite in *pif*Δ *Saccharomyces cerevisiae* cells in a manner dependent on HRR (8). G4 ligands can also induce genome instability showing specific gene interactions in different cell systems. For instance, the compound TMP_yP4, known to bind to telomere G4s, has been shown to enhance murine telomere fragility in the absence of RTEL1, a factor regulating the disassembly of telomeric T loops (a lasso-like telomere organization) (9). Recent work has shown that G4 structures can cause a high rate of sister chromatid exchange in Bloom helicase (*BLM*)-mutated cells derived from Bloom syndrome patients (10). The authors proposed that *BLM* preserves genome stability by resolving G4 structures and suppressing recombination at transcribed genomic loci. Thus, stabilization of G4s by specific ligands or genetic defects can lead to genome instability through the induction of DSB and/or activation of recombination repair pathways. Nevertheless, the mechanism of DSB formation and genome instability by G4 ligands is unknown.

A G4 can be structurally compatible with an R loop, which is another noncanonical secondary DNA structure wherein the two strands of a DNA duplex are separated and one of them is annealed to an RNA, forming a DNA:RNA hybrid (11–14). G4s were shown to form in the displaced strand of an R loop, forming a G loop, depending on high transcription rate and negative supercoiling of

Significance

In the past decades, several compounds have been developed specifically targeting G quadruplexes (G4s), as these noncanonical DNA structures are considered promising targets of effective anticancer drugs. However, despite the high number of known ligands, none showed efficacy in cancer patients. We have investigated the interplay of G4s with R loops, another noncanonical DNA structure, and the findings reveal a mechanism of genome instability and cell killing by G4 ligands, particularly effective in cancer cells deficient of *BRCA2* activity. This knowledge establishes a mechanistic model of G4 ligand activity in cancer cells that can open new lines of investigation aiming at developing clinically effective G4 ligands.

Author contributions: G.C. conceived the research; A.D.M., S.G.M., O.S., and G.C. designed research; A.D.M., S.G.M., M.R., J.M., and R.M. performed research; A.D.M., S.G.M., M.R., J.M., O.S., and G.C. analyzed data; and G.C. wrote the paper.

The authors declare no conflict of interest.

This article is a PNAS Direct Submission.

Data deposition: The data reported in this paper have been deposited in the Gene Expression Omnibus (GEO) database, https://www.ncbi.nlm.nih.gov/geo (accession no. GSE115957).

[1]A.D.M. and S.G.M. contributed equally to this work.

[2]Present address: Department of Oncology, Hematology and Rheumatology, University Hospital Bonn, 53127 Bonn, Germany.

[3]Present address: Division of Gene Regulation, Netherlands Cancer Institute, 1066 CX Amsterdam, The Netherlands.

[4]To whom correspondence should be addressed. Email: giovanni.capranico@unibo.it.

This article contains supporting information online at www.pnas.org/lookup/suppl/doi:10.1073/pnas.1810409116/-/DCSupplemental.

Published online December 27, 2018.

the DNA template (15). The structural compatibility of G4s and R loops is consistent with the knowledge that the formation of both G4s and R loops is favored by similar DNA structural aspects, such as G richness of displaced strands and negative torsional tension, which are common features of active gene promoters (16–18). Interestingly, R loops play a role in several physiological functions of cells; however, unscheduled R loops can lead to DSB, genome instability, and cell killing (12, 13, 19).

Thus, we have here investigated the effects of G4 ligands on R-loop formation and genome integrity in human cancer cells. By studying three structurally unrelated G4 ligands and an inactive analog, our findings establish that G4 ligands induce an immediate increase of nuclear R loops that mediate the formation of DSB. We also discovered that G4 ligands cause the generation of micronuclei at later times in an R loop-mediated manner, particularly in *BRCA2*-depleted cancer cells. Our findings establish a mechanistic role for R loops in mediating the cellular effects of G4 ligands, and open unexpected lines of investigation and development of new anticancer strategies.

Results

G4 Ligands Induce an Increase of Nuclear DNA:RNA Hybrid Structures. We set out to define the interactions of G4s with R-loop structures in relation to genome integrity in human U2OS cancer cells. We first determined with immunofluorescence microscopy (IF) the induction of DNA:RNA hybrids by three established and structurally different G4 ligands: pyridostatin (2), Braco-19 (2), and FG (compound **1** in refs. 20 and 21) (*SI Appendix*, Fig. S1*A*). Nuclear G4s and hybrids were visualized with BG4 and S9.6 antibodies, respectively, validated previously (21) or with specific assays (*SI Appendix*, Fig. S1 *B–G*). In particular, our high-stringency buffer conditions prevented the binding of S9.6 Ab to the cytoplasm, as we rarely detected cytoplasmic signals (Fig. 1; see also *SI Appendix*, Figs. S1, S3, and S4). G4 ligands robustly increased the number of nuclear G4s and hybrid foci between 2 and 10 min in U2OS cells, whereas they dropped close to baseline levels or lower at later times (30 to 60 min; Fig. 1 *A* and *B*). The kinetics of hybrid and G4 formation paralleled each other closely (Fig. 1*B*), and increased hybrids were located in the nucleoplasm, clearly outside the nucleolus, as visualized with nucleolin staining, indicating that they were not restricted to highly transcribed ribosomal RNA genes (Fig. 1*A*). The transient increase of G4s and hybrids at short times was specific, as an FG analog, FA (*SI Appendix*, Fig. S1*A*), which did not stabilize G4s in vitro and in living cells (compound **3** in ref. 20 and compound **14a** in ref. 21), did not increase hybrids either (Fig. 1 *A* and *B*). We must note that FA is more cytotoxic than FG (21) (see below), and thus the mechanism of action of the former is likely different from the latter.

As G4 focus stabilization by specific ligands was often reported to occur after 24 h (1, 2), we also tested these conditions and showed that PDS and FG, but not FA, also induced both G4 and

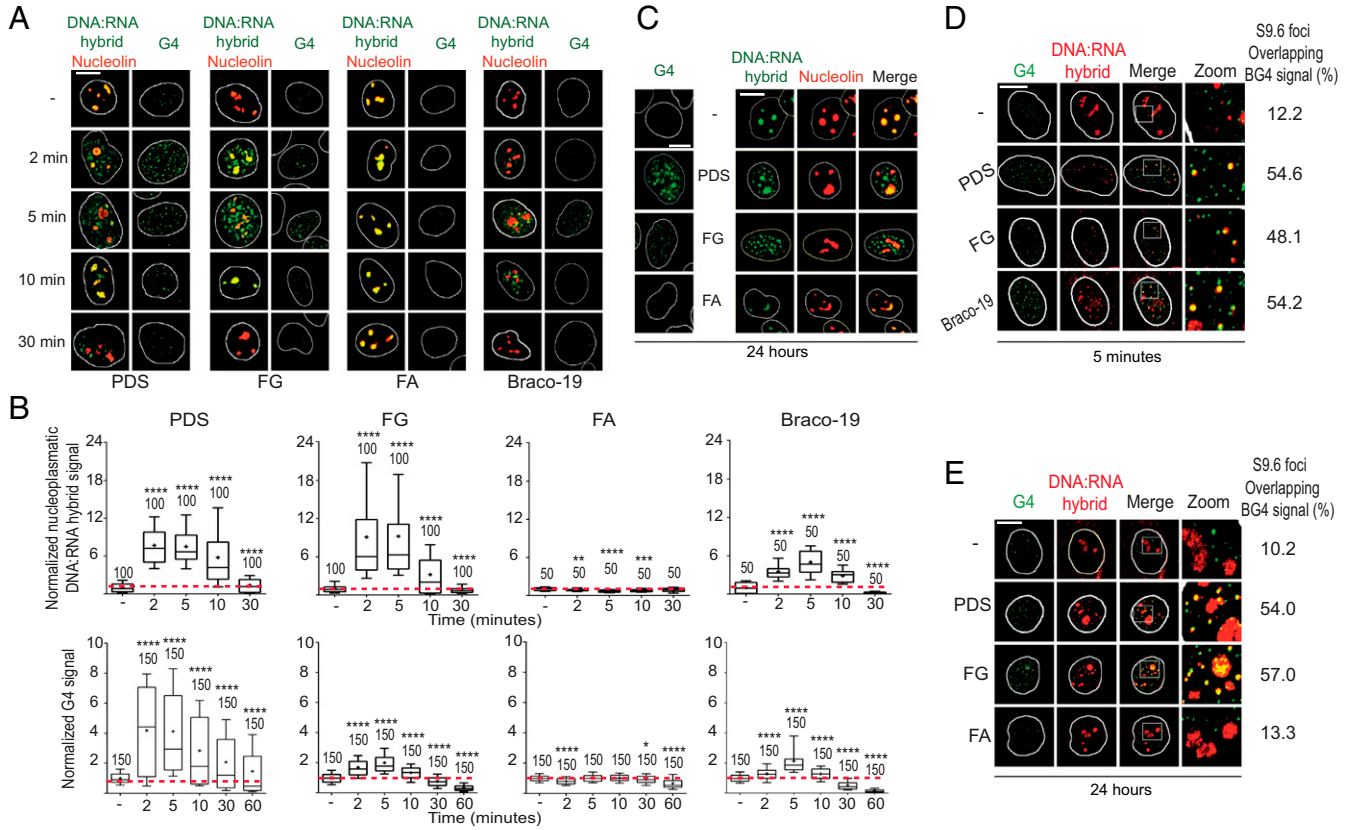

Fig. 1. G4 binders induce nuclear DNA:RNA hybrids overlapping G4 foci. (*A*) Human U2OS cells were treated with PDS, FG, FA (10 μM), or Braco-19 (15 μM) for the indicated times. IF images were analyzed after labeling G4s, hybrids, and nucleolin with BG4, S9.6, and AB22758 antibodies, respectively (as indicated by color). White lines indicate nuclei. (*B*) Hybrid and G4 levels were determined by fluorescence intensity (FI) of cells treated as in *A*. FI of the nucleoplasmic compartment was calculated by subtracting the nucleolar signal from total nuclear FI. The graphs show FI levels normalized over untreated cells of two biological replicates, and numbers indicate analyzed nuclei. Boxplots are as detailed in *SI Appendix, Methods*; horizontal lines and plus signs are median and mean values, respectively. Asterisks indicate statistical significance in comparison with untreated cells by the Kolmogorov–Smirnov parametric test. $*P < 0.05$, $**P < 0.01$, $***P < 0.001$, $****P < 0.0001$. (*C*) G4 foci and hybrid signals induced by 24-h treatments with 10 μM PDS, FG, or FA. U2OS cells were stained as in *A*. Hybrid and G4 levels are shown in *SI Appendix*, Fig. S2C. (*D*) Colocalization of hybrid signals with G4 foci. Cells were treated as in *A* for 5 min and then stained with BG4 (green) and S9.6 (red) antibodies. (*E*) Colocalization of hybrid signals with G4 foci as in *D*, but cells were treated for 24 h. (Scale bars, 10 μm.)

hybrid foci at 24 h (Fig. 1*C*). As we reported that the topoisomerase I (Top1) poison camptothecin can transiently enhance nuclear DNA:RNA hybrids at short times in cancer cells (22), we wondered whether FG and PDS can also poison Top1. We then measured Top1–DNA cleavage complexes in U2OS cells, as described (23). The results showed that PDS and FG are not Top1 poisons (*SI Appendix*, Fig. S2*A*), thus excluding the possibility that Top1 poisoning accounts for the increase of hybrids by the studied ligands. In addition, FG and FA were previously shown to have negligible binding activity toward DNA duplexes (20, 21). Thus, the cellular effects of the studied G4 ligands on hybrid induction are likely due to their specific G4 binding activity. In addition, while FG was as effective as PDS in increasing hybrid foci in the nucleoplasm (Fig. 1 *B* and *C*), PDS increased hybrid signals at nucleoli more than FG and Braco-19 (*SI Appendix*, Fig. S2 *B* and *C*). These observations therefore suggest that PDS, Braco-19, and FG may differently affect R loops along the genome of U2OS cells, likely due to binding to different sets of G4 targets.

Further investigations of the kinetics and dose dependence of hybrid and G4 formation by PDS, Braco-19, and FG showed that the increase of hybrids observed from 2 to 10 min was followed by several hours (0.5 to 6) with no induction, and then by a second increase at 18 to 24 h (*SI Appendix*, Fig. S3 *A*–*E*). In addition, hybrid induction was clearly dose-dependent for PDS and Braco-19 (*SI Appendix*, Fig. S3 *F* and *G*). We noted, however, that Braco-19 had somewhat different kinetics at 18 to 24 h in comparison with PDS and FG (*SI Appendix*, Fig. S3 *B* and *E*), suggesting different cellular outcomes among the compounds.

As the induction of hybrids was always coupled to increased G4 foci, our IF data are consistent with a direct effect of ligand-stabilized G4s on R-loop formation and/or stability. Moreover, the observed biphasic kinetics supports that nuclear R loops are highly dynamic structures (24), likely regulated by homeostatic mechanisms. In this context, G4 stabilization may act as a favoring factor that would, however, stimulate a counterbalancing factor that will then reduce R-loop levels. For instance, unscheduled R loops are expected to inhibit transcription, which would then disfavor the formation of G4s and R loops after the initial increase. Thus, we wondered whether G4s and R loops were localized in the same chromatin domain, and then performed colabeling confocal IF experiments with BG4 and S9.6 antibodies. Interestingly, hybrid signals significantly overlapped with G4 foci in cells treated for short (5 min) or long times (24 h) with PDS, Braco-19, and FG (Fig. 1 *D* and *E*). It must also be noted that several G4 foci did not overlap with hybrids (Fig. 1 *D* and *E*). Within the resolution limits of IF, these observations showed that G4 ligands may stimulate both hybrid and G4 foci at the same or very close chromatin domains and that stabilized G4s may favor a nearby R loop.

Next, we wondered whether G4 ligands can increase R-loop levels in other human cell lines. Since PDS has been shown to be less effective in G4 stabilization in normal cells (1, 25), we also determined G4 ligand effects either in normal human WI-38 and IMR-90 lung fibroblasts or HeLa cancer cells. Interestingly, PDS and FG did not increase G4s nor hybrids at detectable levels in normal WI-38 and IMR-90 fibroblasts at all time points, whereas the ligands increased G4 foci and hybrid signals in HeLa cells after 5-min and 24-h treatments (*SI Appendix*, Fig. S4). Thus, the data may suggest that the studied cancer cells may suffer from a loss of function(s) resulting in a defect in the removal of G4 structures and hence in detectable IF signals. Altogether, our results show that the studied G4 ligands can induce the simultaneous formation of G4 and DNA:RNA hybrid structures at close chromatin domains in the studied human cancer cells.

G4 Ligands Induce R-Loop Spreading into Adjacent Regions Containing Experimentally Observed G4 Structures. To gain insights into the mechanism of R-loop induction by G4 ligands, we wondered whether genomic locations of R loops overlapped with G4 structures, as previously established in human genomic DNA in the presence of PDS with a polymerase-stop assay (26). Thus, we focused on two G4 ligands, PDS and FG, and determined genomic R-loop maps by DRIP-seq (DNA:RNA immunoprecipitation-using sequencing) (18, 27) in U2OS cells treated for 5 min with the compounds to identify the genomic sites of affected R loops. Two biological replicates were performed for untreated and treated cells. To identify specifically the hybrids, we sequenced recovered DNAs from those cell samples that had been left untreated or treated with *Escherichia coli* RNaseH after restriction enzyme digestion and before immunoprecipitation with S9.6 (Fig. 2*A*; see also *SI Appendix*, *Methods*). R-loop peaks were then identified only if they were consistently observed in both replicates and absent in the RNaseH-treated samples. Fig. 2*A* shows a representative gene, TLE3 (Transducin-Like Enhancer of Split 3), which encodes a transcriptional corepressor protein. With these stringent criteria, we obtained thousands of R-loop peaks in control and treated cells covering from 2.5 to 5.1% of the genome (*SI Appendix*, Fig. S5*A*), and each pair of biological replicates showed high correlation coefficients (*SI Appendix*, Fig. S5*B*). R-loop peaks were consistently found in gene regions and were highly enriched at 5′- and 3′-end gene regions (*SI Appendix*, Fig. S5*C*), in agreement with previous findings (18, 24, 27–30). We observed that the profiles of R-loop peaks were highly correlated with each other, and genomic peak distributions were very similar between control and treated cells (*SI Appendix*, Fig. S5 *D* and *E*). However, the peak number and genome coverage were higher for treated than control cells (*SI Appendix*, Fig. S5*A*), suggesting an increase of R loops by the two ligands without alterations of global patterns of genomic R loops.

As the observed genomic increase can be due to higher R-loop levels at specific regions or to the spreading of preexisting peaks, we then investigated both possibilities. A direct comparison of peak intensity showed a high number (97%) of increased peaks (gain), whereas decreased peaks (loss) were only few (FG: 4,411 gain and 149 loss; PDS: 9,881 gain and 272 loss). Gain peaks were particularly enriched at the 3′ end of genes (Fig. 2*B*), but we did not observe a significant enrichment of experimentally observed G4 motifs (26) with gain peaks compared with unchanged peaks. However, as R loops and G4s have been associated with active transcription and promoters (18, 27, 28, 31), we then measured gene expression levels in control cells by RNA-seq to determine transcription-dependent effects of G4 ligands on R-loop levels. Then, we divided genes into four classes depending on transcription levels, and calculated the increase of DRIP sequence reads induced (as Δ reads) by PDS and FG at their transcription start sites for each expression category (Fig. 2*C*). The results show that the increase of DRIP reads is highly correlated with transcription levels and the presence of CpG islands, thus suggesting that both transcription and guanine-rich sequences can favor the increase of R loops, likely due to a prompt binding of the ligands to their targets at active and accessible promoters. Moreover, we wondered whether GC skew (G richness on the nontranscribed strand) could affect R-loop increase by the studied G4 ligands. The data show that the studied ligands increased DRIP reads at higher levels in actively transcribed CpG-island promoters with GC skew than in those without GC skew (*SI Appendix*, Fig. S5*F*), further supporting a critical role for ligand binding to G4 targets at active promoters.

Next, as we noticed that R-loop peaks were often shared between control and G4 ligand-treated cells (see instances in Fig. 2*A*), we wondered whether gains were due to extended R loops more than to higher peak intensity. Thus, we analyzed the length of common peaks (more than 13,000 for each compound) and found that a significant number of them were extended by PDS and FG (Fig. 3*A*). Interestingly, extended peaks were enriched particularly at gene 3′ ends for both G4 ligands (Fig. 3*B*). This indicated that G4 ligands could frequently induce R-loop

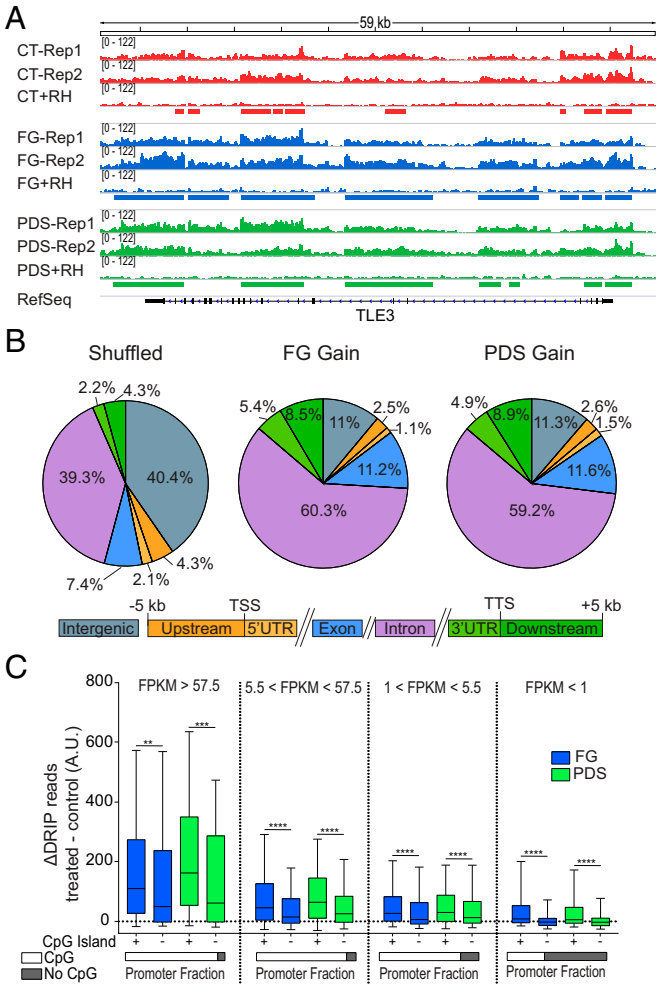

Fig. 2. G4 binders increase R-loop levels at CpG-island promoters of transcribed genes. (*A*) Genomic R-loop profiles at the TLE3 gene locus. Two biological replicates are shown for either control or G4 binder-treated cells along with an RNaseH-treated sample. Control cells are red; cells were treated with FG (blue) or PDS (green) for 5 min. Rectangles indicate R-loop peaks. (*B*) Distribution of DRIP peak gains for FG (*Middle*) and PDS (*Right*) across the genomic compartments depicted below. Numbers indicate the percentage occupied by each compartment. (*B*, *Left*) The graph shows the compartment distribution of randomly shuffled peaks over the full genome. TSS, transcription start site; TTS, transcription termination site. (*C*) Increased DRIP read counts at active promoter TSSs are dependent on the transcription level and the presence of CpG islands. Analyzed regions are from 2,000 bp upstream to 2,000 bp downstream of the TSS. Genes are split into four categories based on transcript levels as established by RNA-seq data and indicated at the top of the graphs. FPKM, fragments per kilobase of gene exon model per million reads mapped. As indicated below, TSS promoters with CG islands constitute 92.9, 90.6, 81.8, and 37.4% for the four gene sets from left to right, respectively. Statistical significance was determined with the Kolmogorov–Smirnov test. $^{**}P < 0.01$, $^{***}P < 0.001$, $^{****}P < 0.0001$.

spreading to adjacent regions. Thus, to understand whether R-loop spreading was associated with nearby G4s, we determined the overlapping between extended peak regions and experimentally observed G4 structures (26), focusing on extended peaks with a fold change >1.5 and $P < 0.05$ (1,000 and 619 for FG and PDS, respectively; red asterisks, Fig. 3*A*). To take into consideration the strand forming the G4 or the hybrid, we considered that the observed G4 dataset is constituted by over 700,000 G4 sequences assigned to one of the two genomic strands (26). Then, we assigned DNA:RNA hybrids mapped at transcribed genes to the template strand of genes (*SI Appendix*, *Methods*). As R-loop peaks are frequent in GC-rich sequences (Fig. 2*C*), we also selected peaks not extended by G4 ligands (unchanged; blue dots, Fig. 3*A*) and matched to extended peaks for length and gene localization to be compared with extended peaks. Then, we calculated the enrichment of observed G4s at extended and unchanged peaks relative to random peaks (*SI Appendix*, *Methods*). The results showed that G4s in the displaced strand of R loops were more enriched in extended peaks than unchanged peaks (darker vs. lighter colors, Fig. 3*C*) for both PDS and FG, whereas G4s in the template strand were not enriched (Fig. 3*C*). Interestingly, FG-extended peaks show a significant depletion of extensions without any G4 (Fig. 3*C*). Thus, the statistical analyses suggest that G4 ligands can induce R-loop spreading when G4 structures are present in the displaced strand of adjacent regions. A comparison of extended peaks by FG and PDS showed that 248 peaks only were in common between the two ligands, while a large fraction of them were ligand-specific (57 to 74%; Fig. 3*D*), supporting a degree of ligand binding specificity to distinct genomic sets of G4 targets. To validate the bioinformatic analyses and R-loop spreading, we performed DRIP-qPCR determinations of R-loop levels at 15 extended peaks in cells treated with PDS and FG for 5 min. All of the tested regions with one exception (*VSIG8* gene for PDS) showed an increase of R-loop levels by the two ligands (Fig. 3*E*). Thus, altogether, these findings provide evidence that a G4 structure in the displaced strand of an R loop can likely stabilize and extend the overall structure when bound by specific ligands in cancer cells.

G4 Ligand-Induced DNA Damage Is Mediated by R Loops. As the studied G4 ligands can stabilize G4s along with R loops in nuclear chromatin of human cancer cells, we next investigated the biological consequences of R-loop induction. In particular, as G4 ligands are known to induce DNA damage and genome instability (1, 2), we asked whether this is due to increased levels of R loops.

First, we assessed the induction of DNA damage by PDS and FG in U2OS cells. Following 24 h of treatment, the two ligands induced an increase of S139-phosphorylated histone H2AX (γH2AX) foci (Fig. 4*A*) and of G2/M cells (*SI Appendix*, Fig. S6*A*), which are both hallmarks of genomic DSB and DDR. Moreover, we detected a marked increase of foci of 53BP1 (p53-binding protein 1) and S1778-phosphorylated 53BP1 (p53BP1; a specific marker of DSB and DDR activation) in cells treated with PDS for 24 h (Fig. 4 *B* and *C* and *SI Appendix*, Fig. S6*B*). Interestingly, p53BP1 foci showed a nearly perfect colocalization with γH2AX foci (Fig. 4*B*). DNA damage checkpoint activation was also assessed by measuring the induction of pATM (S1981-phosphorylated ATM; a marker of DDR activation) by PDS after 24-h treatments (Fig. 4 *B–D* and *SI Appendix*, Fig. S6*C*). Interestingly, pATM foci fully colocalized with γH2AX foci (Fig. 4*B*), indicating ATM recruitment to chromatin sites of DSB. FG and FA have minor effects on the levels of p53BP1 and pATM foci at 24 h (Fig. 4*D*, *Left* and *SI Appendix*, Fig. S6 *B–E*). However, the ratio pATM/ATM was increased by PDS and FG, but not FA, after 24 h (Fig. 4*D*, *Right*), suggesting that DDR is activated after 24 h with PDS as well as FG.

Then, as G4 ligands increased hybrid levels after 2 to 10 min (see above), we measured γH2AX focus levels at shorter times. γH2AX foci were consistently increased around twofold by PDS and FG after 1 to 4 h of treatment (Fig. 4*E*), in agreement with a published report on PDS (5), showing that the increase of unscheduled R loops preceded γH2AX focus formation. Interestingly, the γH2AX kinetics of PDS was markedly different from that of FG (Fig. 4*E*). In response to PDS, γH2AX focus number increased progressively over 24 h whereas, in response to FG, γH2AX foci reached a plateau after 2 to 4 h and then decreased somewhat after 20 to 24 h (Fig. 4*E*). FA, which did not induce G4s and R loops (see above), was slightly effective at inducing γH2AX, but less than FG (Fig. 4 *A*, *D*, and *E*). Braco-19

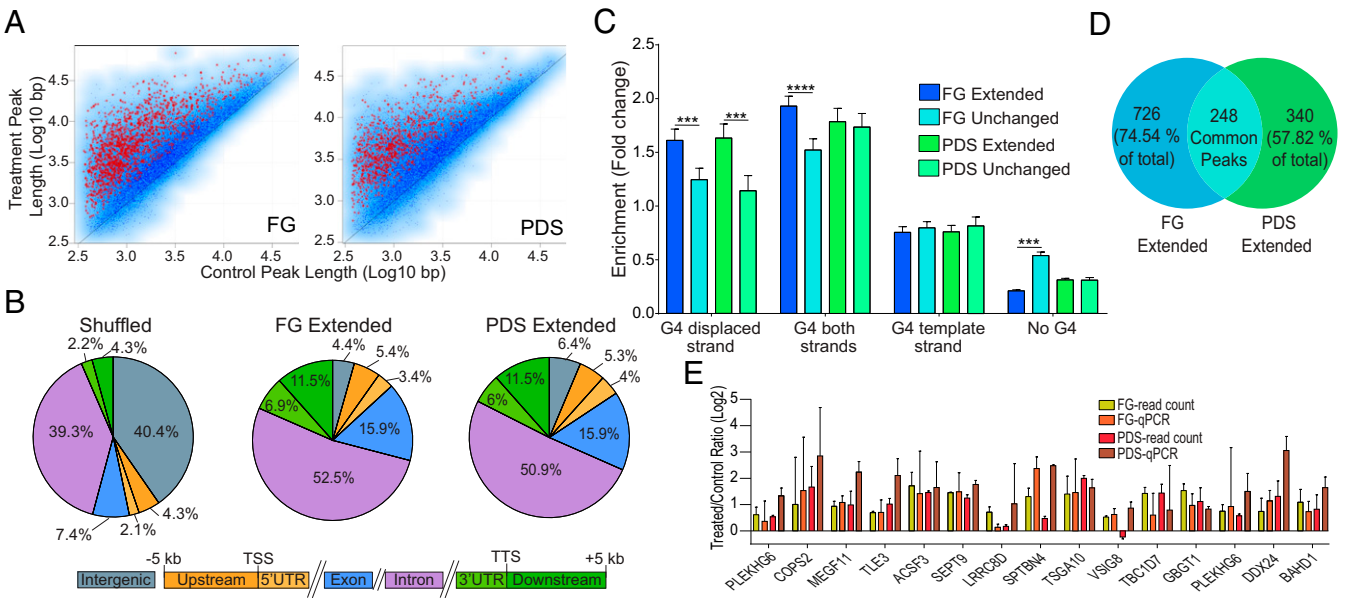

Fig. 3. G4 binders extend R loops at adjacent regions enriched for G4 motifs in the displaced strand. (*A*) Scatter plots of R-loop lengths of common peaks (13,539 and 13,316 for FG and PDS, respectively) between untreated and G4 binder-treated cells. Extended peaks with a length fold change >1.5 and $P < 0.05$ (red asterisks) are 1,000 and 619 for FG and PDS, respectively. Peaks with a length fold change <0.66 and $P < 0.05$ (not highlighted) are 8 and 14 for FG and PDS, respectively. Tests used were the *t* test and robust moderated *t* test from the limma R package (*SI Appendix, Methods*). (*B*) Distribution of DRIP extended peaks for FG (*Middle*) and PDS (*Right*) across the genomic compartments depicted below. Numbers indicate the percentage occupied by each compartment. (*B*, *Left*) The graph shows the compartment distribution of randomly shuffled peaks over the full genome. (*C*) Enrichments of experimentally established G4 motifs (29) in extended regions of extended peaks (red asterisks in *A*) in comparison with unchanged peaks (blue dots in *A*), matched to extended peaks for length and genomic localization. Extended peaks in genic regions only were considered for the analysis (974 for FG, 588 for PDS). Test used: Kolmogorov–Smirnov test. ***$P < 0.001$, ****$P < 0.0001$. (*D*) Venn diagram showing peak overlap between genic extended peaks for FG and PDS. (*E*) R-loop levels measured by DRIP-qPCR and DRIP-seq read count at 15 extended peaks. DRIP-qPCR measurements and DRIP-seq read count measurements in the same amplicon regions are shown as fold changes (treated over control). Bars show means ± SEM of four determinations from two experiments. Recovery of R loop-negative regions is around 100-fold less than positive loci (*SI Appendix*, Fig. S1).

also increased γH2AX foci, with a kinetics similar to that of PDS (*SI Appendix*, Fig. S6*F*). As G4 ligands did not stabilize G4s and hybrids in normal WI-38 fibroblasts (*SI Appendix*, Fig. S4), we also determined γH2AX levels in these cells. Consistently, G4 ligands did not induce γH2AX in WI-38 fibroblasts (*SI Appendix*, Fig. S6*G*).

Next, we asked whether DSB induced by G4 ligands is mediated by unscheduled R loops. To this end, we used a U2OS cell line which has stably been transfected with a vector expressing an mCherry-RNaseH1 under the control of a doxycycline (Doxy)-inducible Tet promoter (*SI Appendix*, Fig. S7*A*) (32). PDS induced a 1.8- to 2.1-fold increase of γH2AX foci in cells not expressing the enzyme, whereas PDS induced a 0.83-fold change in cells overexpressing mCherry-RNaseH1 (Fig. 4 *F* and *G*). The results demonstrate that RNaseH1 overexpression fully prevented the induction of γH2AX foci by PDS. Interestingly, PDS and FG induced low levels of G4 foci in cells overexpressing mCherry-RNaseH1 at short times, suggesting that RNaseH1 overexpression can prevent a full stabilization of G4 structures by the studied ligands (*SI Appendix*, Fig. S7*B*). Altogether, the results thus support that G4 ligand-induced DNA damage is mediated by unscheduled G4/R-loop structures.

To understand whether R-loop induction has any consequence on cell death induced by the studied G4 ligands, we determined the cytotoxic activity of PDS, FG, and FA in U2OS and U2OS_RH cells, the latter being a cell line stably transfected with a FLAG-tagged human RNaseH1 gene under a doxycycline-inducible Tet promoter (*SI Appendix*, Fig. S8*A*). Cell-killing activity of FG was reduced in U2OS_RH cells compared with U2OS cells, and the reduction was stronger when RNaseH1 was overexpressed by doxycycline, whereas cell-killing activity of FA was essentially unaffected (Table 1). PDS data were not meaningful, as it was poorly cytotoxic (Table 1). As FA did not increase G4s and R loops (Fig. 1) and is even more cytotoxic than FG, its mechanism of action is independent of the studied noncanonical DNA structures. Thus, overall, the findings support a main role for R loops in the induction of DNA damage and cell killing by the studied G4 ligands in human cancer cells.

G4 Ligand-Induced DNA Damage Is Mediated by R Loops in *BRCA2*-Depleted Cancer Cells. As G4 ligand-induced DSB can be repaired by HRR mechanisms and *BRCA2*-deficient cells are more sensitive to G4 ligands (6, 7), we wondered whether the hypersensitivity of HRR-deficient cells to G4 ligands was dependent on R loops. Therefore, we first determined whether the HRR pathway is activated in U2OS cancer cells by assessing foci formation of Rad51, a factor involved in the essential strand-invasion step of the HRR pathway (33, 34). IF results showed a consistent increase of Rad51 foci by 24-h treatments with PDS and FG, but not FA, to a very similar extent (Fig. 4*H* and *SI Appendix*, Fig. S8*B*), indicating an activated HRR in U2OS cells. Then, to establish the role of R loops in HRR-deficient cells, we silenced the *BRCA2* gene with siRNA in both U2OS and U2OS_RH cell lines (Fig. 5*A* and *SI Appendix*, Fig. S8*C*) and determined the number of γH2AX foci induced by PDS and FG with or without RNaseH1 overexpression.

Surprisingly, the effects of BRCA2 silencing were somewhat different between FG and PDS. In *BRCA2*-silenced U2OS cells, γH2AX focus levels by PDS were increased at early times compared with WT cells (from 1.26 to 1.54 fold change at 1 h, and from 1.98 to 2.69 fold change at 4 h) (Fig. 5*B* and *SI Appendix*, Fig. S9*A*). In contrast, the kinetics of γH2AX by FG was not altered and the levels of γH2AX foci were even somewhat reduced by *BRCA2* silencing (Fig. 5*C* and *SI Appendix*, Fig. S9*B*). Next, as γH2AX foci were increased at early times, we determined the

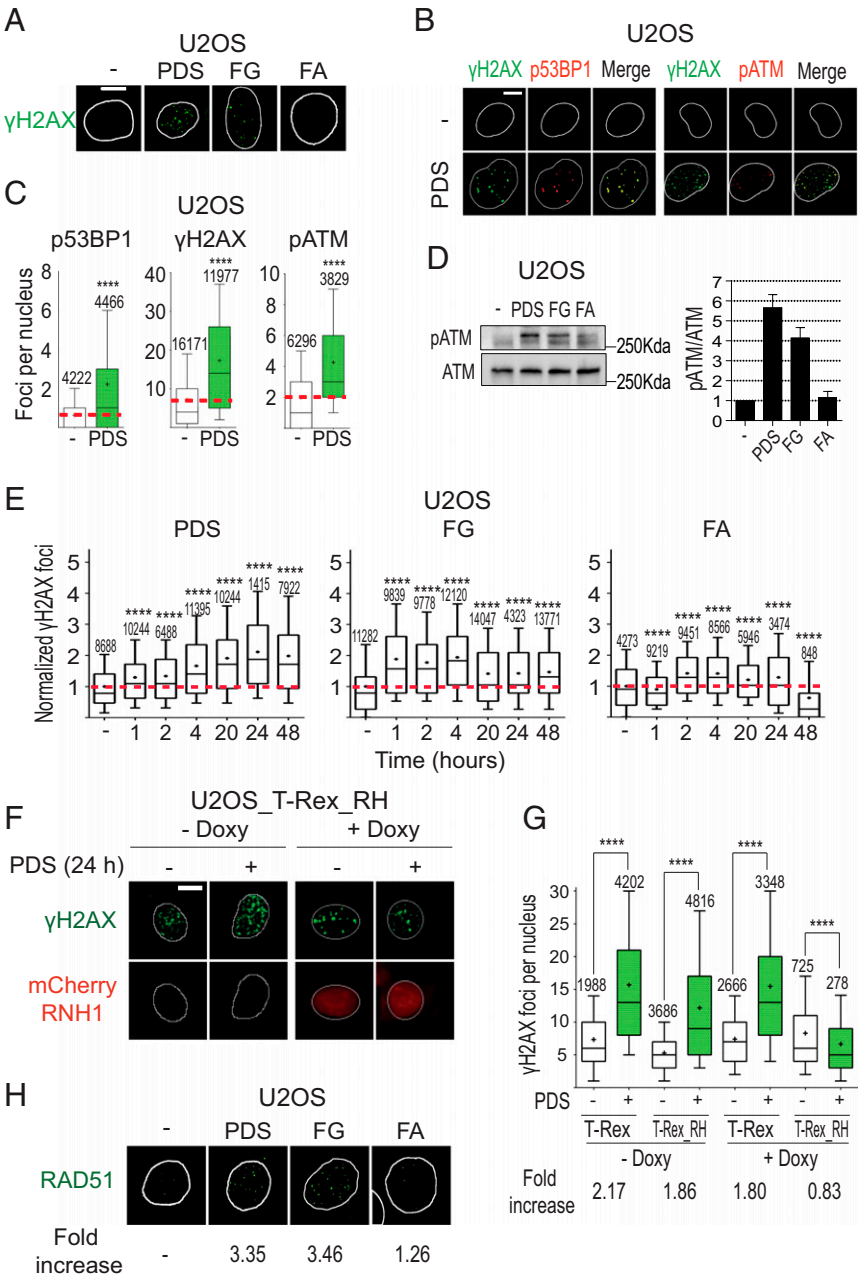

Fig. 4. PDS and FG induce DNA damage in an R loop-dependent manner. (*A*) γH2AX (S139-phosphorylated H2AX) foci induced by 10 μM PDS, FG, and FA following 24-h treatments. (*B*) Colocalization of γH2AX foci with p53BP1 (S1778-phosphorylated 53BP1) or pATM (S1981-phosphorylated ATM) foci in cells treated with 10 μM PDS for 24 h. Cells were costained for γH2AX (green) and p53BP1 (red) (*Left*), and for γH2AX (green) and pATM (red) (*Right*). (*C*) Levels of γH2AX, p53BP1, and pATM signals in cells treated as in *B*. (*D*) Western blots of pATM and ATM after 24-h treatments with 10 μM compounds (full membrane is shown in *SI Appendix*, Fig. S6*C*). (*D*, *Right*) Levels of the pATM/ATM ratio after treatment with the indicated compound. The graph shows mean values with standard errors of three biological replicates. (*E*) γH2AX focus levels in U2OS cells treated with the indicated compounds and for the indicated times. (*F*) PDS-induced γH2AX foci in cells expressing an exogenous RNaseH1. T-REX (control vector) and T-REX_RH (RNaseH1-expressing vector) stably transfected U2OS cells were treated with 10 μM PDS for 24 h with or without doxycycline, which activates RNaseH1 expression. RNaseH1 was fused to an mCherry tag to visualize cells with expressed enzyme. (*G*) γH2AX levels in T-REX and T-REX_RH cells treated (green bars) or not (white bars) with PDS as in *F*. Fold increase shows ratios of γH2AX levels in PDS-treated cells over corresponding untreated cells. (*H*) RAD51 foci induced by the indicated compounds (10 μM) after 24-h treatments of U2OS cells. (Scale bars, 10 μm.) All graphs show data from at least two biological replicates, reported as detailed in the legend to Fig. 1*B*. Asterisks indicate statistical significance in comparison with untreated cells by the Kolmogorov–Smirnov parametric test. ****$P < 0.0001$. (Magnification: *H*, 63×.)

induction of γH2AX foci following a 4-h treatment with the studied G4 ligands in U2OS_RH cells upon RNaseH1 expression by doxycycline. Similar results were observed in *BRCA2*-silenced and WT U2OS_RH cells in the absence of doxycycline (Fig. 5*D*, from 1.36 to 1.53 fold change; Fig. 5*E*, from 3.44 to 1.34 fold change), further supporting a difference in γH2AX induction between the two G4 ligands. However, exogenous RNaseH1 expression abolished the induction of γH2AX foci by either G4 ligands in *BRCA2*-silenced or WT cells (Fig. 5 *D* and *E*, + Doxy), showing a complete rescue of DSB. Thus, the findings strongly support that R loops play a main role in DSB induction by PDS and FG also in *BRCA2*-silenced cells regardless of any

Table 1. Exogenous RNaseH1 overexpression reduces cell-killing activity of FG but not FA

Compound	IC_{50}, μM*		
	U2OS	U2OS_RH	U2OS_RH + Doxy
FG	15.9 ± 1.2	52.8 ± 1.1	92.8 ± 1.1
FA	6.77 ± 1.4	7.10 ± 1.3	7.12 ± 1.3
PDS	>50	>50	>50

*Compound concentration inhibiting 50% of cell growth (see *SI Appendix, Methods*). Cells were exposed to the indicated compound for 24 h, and cell survival was determined after a further 48 h in drug-free medium. Numbers are means ± SD of two biological replicates, each performed in triplicate.

different molecular activity of the two ligands. In addition, the data suggest that the reported hypersensitivity of HRR-deficient cells to G4 ligands (6, 7) may be due to unscheduled R-loop formation.

PDS Induces Micronuclei Mediated by R-Loop Formation. During the course of this work, we observed that the studied G4 ligands could increase micronuclei, a clear hallmark of genome instability (35). As genome instability has been linked to impaired regulation of G4 structures in living cells (1, 8, 10, 36), we then asked whether micronucleus induction was mediated by DNA damage and R-loop/G4 structures. First, we investigated micronucleus induction in U2OS cells, showing that PDS increased the fraction of cells with micronuclei to a greater extent in *BRCA2*-silenced than *BRCA2* WT cells (Fig. 5*H* and *SI Appendix*, Fig. S9*C*), suggesting that the observed increase of DSB at early times (Fig. 5*B*) may lead to enhanced formation of micronucleated cells at later times. PDS-induced micronuclei were of different size (*SI Appendix*, Fig. S9 *C* and *D*), found in cytoplasmic regions close to the nucleus, and often showing IF signals of γH2AX (Fig. 5*G*), similar to recent reports using ionizing radiation (37–39). To better characterize micronucleus generation, we performed a cotreatment of PDS with a DNA-PK inhibitor, which fully abolished micronucleated *BRCA2*-silenced and WT U2OS cells (*SI Appendix*, Fig. S9 *E* and *F*) while maintaining a high level of γH2AX foci (*SI Appendix*, Fig. S9*G*), consistent with a strong inhibition of DNA repair. In agreement with previous reports (37–39), as the DNA-PK inhibitor can potentiate a cell-cycle G2/M arrest due to DNA-repair inhibition, the results showed that PDS can trigger micronuclei when PDS-induced DSB fails to be properly repaired and cells transit through mitosis.

We then determined whether micronucleus generation was related to unscheduled R loops. Interestingly, RNaseH1 overexpression in U2OS_RH cells abolished PDS induction of micronuclei in WT cells (from 1.57- to 0.74-fold; Fig. 5*I*) while reducing it in *BRCA2*-silenced cells (from 2.23- to 1.59-fold; Fig. 5*I*). Therefore, RNaseH1 could fully rescue micronucleus formation by PDS in WT cells but only partially in *BRCA2*-silenced cells. However, we noted that *BRCA2* silencing itself increased micronucleated cells (for instance, from 10.4 to 22.4% in untreated U2OS_RH cells without Doxy; Fig. 5*I*), and RNaseH1 overexpression somewhat affected micronucleus numbers as well (Fig. 5*I*). These observations may suggest that DNA repair or mitotic mechanisms of micronucleus generation may involve DNA:RNA hybrid formation, the removal of which might have an opposite effect on PDS-triggered micronuclei.

In contrast to PDS, FG increased the number of cells with micronuclei only slightly (*SI Appendix*, Fig. S10), suggesting that FG-induced DSB largely leads to a different molecular outcome such as cell-killing activity (Table 1). In addition, the slight induction of micronuclei did not allow establishing a clear effect by RNaseH1 overexpression on FG-induced micronuclei (*SI Appendix*, Fig. S10). Thus, the results show that PDS-induced DNA breaks are particularly prone to trigger micronuclei in a manner dependent on unscheduled R loops and G4 structures in *BRCA2* WT and, partially, in *BRCA2*-depleted cancer cells.

Discussion

R loops form abundantly in mammalian genomes and have been associated with different outcomes such as chromatin patterning, Ig gene recombination, DNA DSB, and genome instability (12, 13, 18, 24, 40, 41). However, how R-loop metabolism is regulated is still largely unknown. The present work provides experimental evidence that G4 structures can modulate the formation of R loops at active genes in eukaryotes. We here demonstrate that the studied G4 ligands induce unscheduled R-loop/G4 structures in human U2OS cancer cells likely by extending cotranscriptional R loops, which mediate the cellular activity of the studied compounds. Interestingly, even though PDS and FG can both increase R loops with similar kinetics, the biological outcome is partially different, in terms of DSB kinetics, genome instability, and cell-killing activity. In addition, we discovered that PDS can promote micronucleus generation in cancer cells in a manner dependent on unscheduled R loops. Our findings establish a molecular mechanism of G4 ligands with the potential to open new perspectives for the discovery and development of effective anticancer ligands.

Immediately upon cell exposure, G4 ligands increase R-loop levels and G4 foci, with a maximum at 2 to 10 min, after which R loops decline to undetectable levels for several hours. This immediate occurrence is likely due to the specific action of the compounds, namely stabilization of G4 structures through direct binding (Fig. 6). Thus, the simultaneous and rapid biphasic kinetics are a specific outcome of the studied G4 ligands in U2OS cells, likely due to a dynamic balance under homeostatic control of G4/R-loop levels. The immediate and rapid kinetics of R-loop/G4 structures may be due to a topological effect of G4 stabilization, as noncanonical DNA structures and DNA-duplex torsional stress may affect each other (16). On the other hand, the subsequent rapid reduction could result from transcription inhibition caused by increased R-loop levels and extensions (Figs. 2 and 3), and/or by active R-loop/G4 structure removal by repair mechanisms or specific helicases (1, 12, 14, 28). However, the mechanistic nature of the observed dynamic balance needs to be established in future work. Genomic maps showed that G4 ligands mainly induced R-loop gains at highly expressed genes, in particular at 5′- and 3′-end gene regions, after 5 min of treatment. The results are consistent with the findings that G4 structures are more often found at open chromatin sites of active genes in untreated cells (42). The reported genomic analyses suggest that PDS and FG can likely extend preexisting R loops to adjacent regions that are enriched for G4-promoting sequences in the displaced, but not template, strand of R loops. As our data are not at single-molecule levels but derive from statistical analyses of several genomic regions, we cannot exclude that increased (extended) R loops may be instead distinct R-loop structures. However, a likely hypothesis is that G4 ligands affect preexisting R loops within minutes of cell treatment, mainly at transcribed regions that are in an open chromatin conformation, in agreement with G4 structures present at these regions in untreated cells (42). Thus, G4 ligands may stabilize preexisting G4 structures in the displaced strand of R loops, in turn stabilizing DNA:RNA hybrids and increasing its length as proposed in our model (Fig. 6), in agreement with the G-loop model shown in *E. coli* (15). However, we believe that distinct mechanisms may be operative at functionally different chromatin regions, leading to reciprocal stabilization of R-loop/G4 structures. Thus, future studies will establish the precise mechanism at specific chromatin regions in living cells.

The increase of unscheduled R-loop/G4 structures can occur at different sets of transcribed genes depending on the specific ligand (Fig. 3*D*). Therefore, although the mechanistic model of

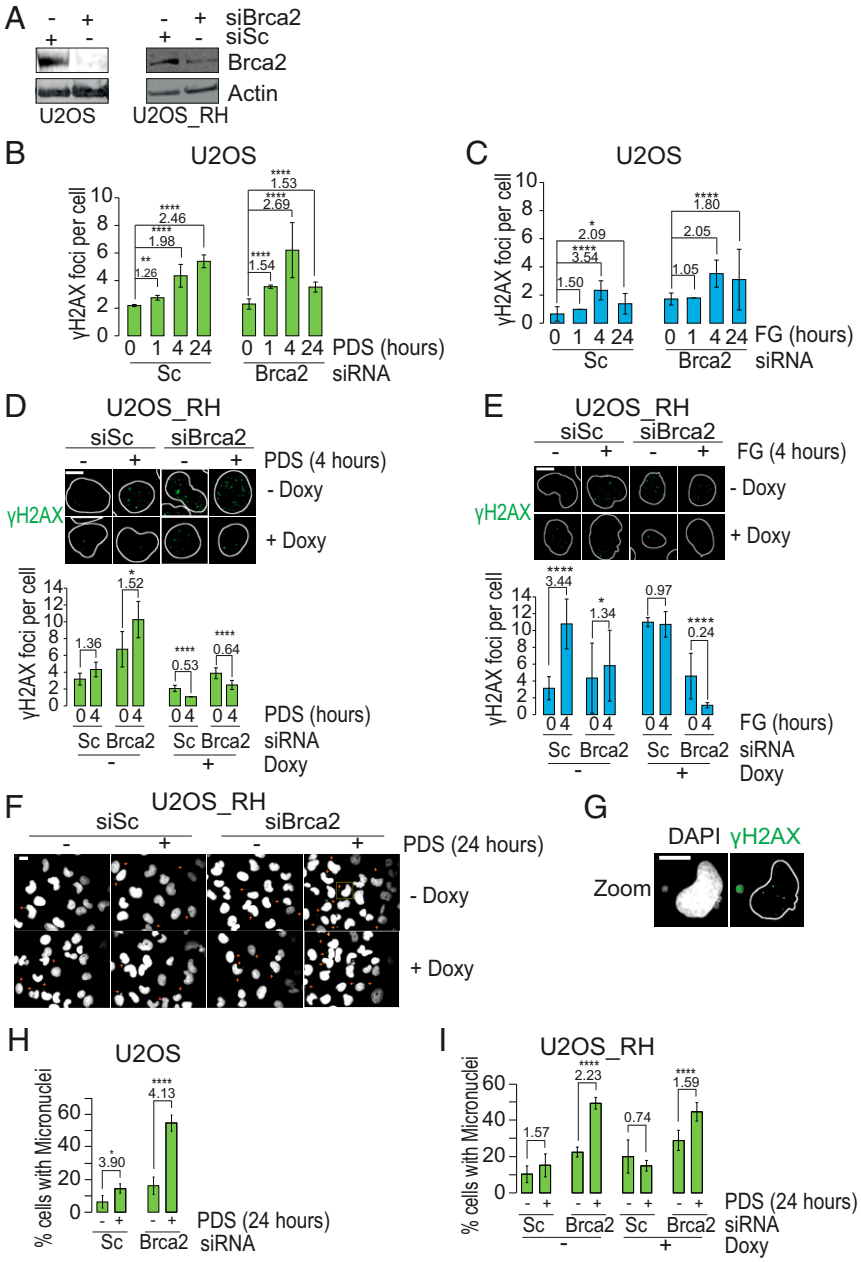

Fig. 5. DNA damage and genome instability are mediated by R loops in *BRCA2*-depleted cancer cells. (*A*) BRCA2 levels in the indicated cells following treatment with the specific siRNA against *BRCA2* (siBRCA2) or scrambled siRNA (siSc) for 48 h (full membranes are shown in *SI Appendix*, Fig. S8*C*). (*B*) γH2AX levels in *BRCA2*-silenced or WT U2OS cells treated with PDS for the indicated times. (*C*) Same as in *B* but cells were treated with FG. (*D*) PDS-induced γH2AX foci in *BRCA2*-silenced cells expressing an exogenous RNaseH1. RNaseH1-expressing vector stably transfected U2OS_RH cells were treated with siBRCA2 or siSc, and then with 10 μM PDS for 24 h with or without doxycycline to activate RNaseH1 expression. RNaseH1 was fused to a FLAG tag to detect the enzyme (*SI Appendix*, Fig. S8*A*). (*E*) Same as in *D* but cells were treated with FG. (*F*) Micronuclei induced in U2OS_RH cells transfected with scrambled siRNA or siRNA against *BRCA2*, and then treated with PDS for 24 h. Small red arrows indicate single micronuclei. (*G*) Enlargement of a cell in the yellow square in *F*. The image shows a micronucleus positive for γH2AX labeling. (*H*) Fractions of U2OS cells with micronuclei with and without *BRCA2* silencing and 24-h treatments with PDS. (*I*) Fractions of U2OS_RH cells with micronuclei with and without *BRCA2* silencing, doxycycline, and PDS treatments as indicated. (Scale bars, 10 μm.) Bars show mean values ± SEM. Fold-increase values are reported above the bars and represent treated/control ratios. Data in all panels are from at least two biological replicates, and in each experiment an average of 250 cells per sample was determined. Statistical significance was determined with the Kolmogorov–Smirnov test performed on the full cell populations. $*P < 0.05$, $**P < 0.01$, $****P < 0.0001$.

R-loop increase by PDS and FG can be similar, the cellular and molecular outcomes can be different depending on the genomic and chromatin context of the increased R loops (Fig. 6). We indeed report a number of differences between PDS and FG, mainly for γH2AX focus kinetics, BRCA2 silencing effects, micronucleus formation, and cell killing. As we used equimolar doses of the studied compounds, resulting in similar cellular levels of R loops (Fig. 1) and γH2AX foci (Fig. 4 *A* and *E*) in U2OS cells, the results show that G4 ligands can have specific molecular effects. Although the findings establish that DSB triggered by PDS and FG is mediated by R loops to a large extent, the described differences suggest that the mechanisms of

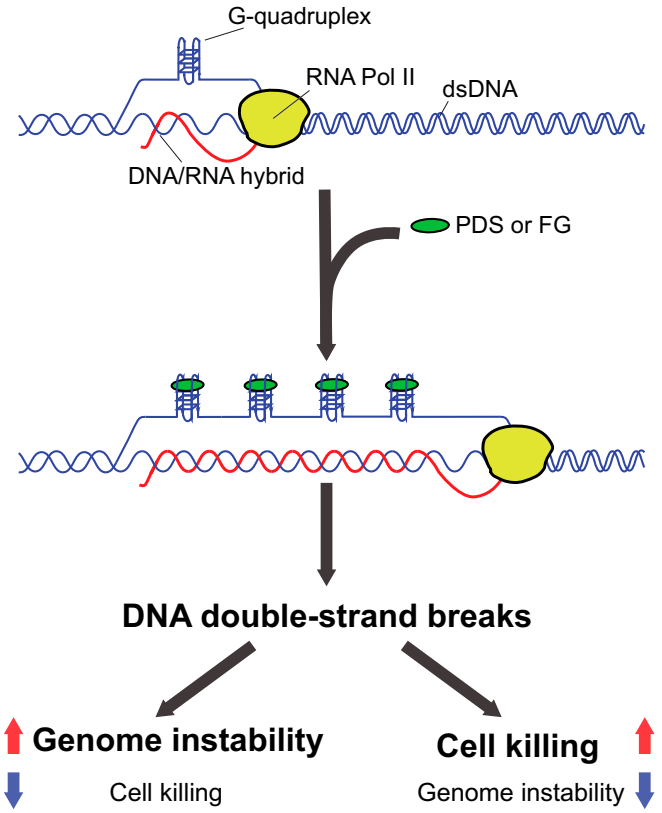

Fig. 6. Molecular model of PDS and FG activity in cancer cells. Ligand-stabilized G4s can cause R-loop spreading at transcribed genes, which results in the accumulation of DNA DSB. DNA breaks can activate molecular pathways leading to either cell killing or micronucleus generation (genome instability).

DNA damage and/or repair may be, at least partially, different. One possibility is that HRR and other DNA repair mechanisms are activated with different strengths and/or chromatin localization of DSB is different for the two studied ligands. Interestingly, active transcription and histone modifications were proposed to regulate DSB repair pathway choice (43, 44). In addition, we cannot completely exclude more selective R loop-independent mechanisms of DNA damage induced by G4 ligands. For instance, the stabilization of G4s in template DNA strands may arrest DNA polymerases triggering replication stress and DNA damage, which may then be resolved by distinct molecular pathways (45). Therefore, it will be interesting to establish in future studies the specificity of DNA damage and repair pathways activated by diverse G4 ligands in relation to stabilized G4s and unscheduled R loops at functionally distinct chromatin sites.

Cooperative interactions between G4s and R loops were previously proposed to occur in *E. coli* and *S. cerevisiae* (15, 36, 46). In particular, the genome instability of a G-rich murine Ig Sμ sequence in yeast was shown to be due to simultaneous formation of G4/R-loop structures under high levels of transcription (36, 46). High transcription levels of the Ig Sμ sequence are required for murine class-switch recombination of Ig genes to likely allow noncanonical DNA structures to form (47). In our study, we found that G4 ligands could trigger cell killing and genome instability with different efficiency. FG was more cytotoxic than PDS, whereas PDS consistently induced micronuclei to a greater extent than FG, particularly in *BRCA2*-depleted cancer cells, with a mechanism involving unscheduled R-loop/G4s and DSB formation (Fig. 6). Micronucleus formation depends on a failure of proper chromosomal DSB repair and requires cell passage through mitosis (35, 37, 38). Interestingly, micronuclei can be a source of cytoplasmic genomic DNA that can activate the STING (stimulator of interferon genes) proinflammation response, eventually leading to activation of the innate immune system (37, 38, 48, 49). Of note, a high frequency of micronucleation was reported in mouse embryonic fibroblasts lacking RNaseH2, a model of monogenic autoinflammation diseases (37, 50). RNaseH2 is an RNaseH enzyme present in mammalian cells, which is involved in ribonucleotide excision repair (51, 52) and can also resolve R loops (11–14). Thus, unscheduled R loops may trigger micronucleus generation in different cell types, and our findings suggest that micronuclei induced by PDS, and to a lesser extent by FG, might lead to an immunostimulatory response in human cancer cells.

Therefore, we have uncovered an R loop-dependent mechanism of DSB accumulation and genome instability caused by the studied G4 ligands in human cancer cells. The mechanistic role played by unscheduled R loops/G4s in the ligand activity can be exploited to discover new anticancer compounds. In addition, our findings foresee the potential of anticancer therapies based on the combination of immunotherapy with G4-targeting small molecules able to elicit an effective innate immune response.

Methods

Compounds. FG and FA were synthesized as described previously (53); IR, ^{1}H NMR, ^{13}C NMR, mass spectral data, and elemental analyses are reported in *SI Appendix, Methods*. Pyridostatin and Braco-19 were purchased from Merck. Chemical reagents were from Merck if not otherwise indicated and were used as indicated in *SI Appendix, Methods*.

Cell Lines. The human U2OS cell line was purchased from ATCC (LGC Standards). Human WI-38 fibroblasts, immortalized with hTERT (54), were kindly obtained from C. Mann (CEA, Gif-sur-Yvette, France) and E. Nicolas (Université de Toulouse). U2OS_T-Rex_RH (expressing an mCherry-tagged RNaseH1) and U2OS_T-Rex cell lines were a kind gift from P. Calsou (IPBS, Toulouse, France), as described already (32). We generated the human U2OS_RH cell line as follows: U2OS cells were first transfected with a pLVX-EF1α-Tet3G-Hygro Tet transactivator-expressing vector and selected with 500 μg/mL hygromycin B. Then, hygromycin-resistant cells were transfected with a pLVX-Tight-Puro vector expressing a FLAG-tagged truncated version of human RNaseH1 (pLVX-Tight-Puro-RH-Flag) and selected with 1.5 μg/mL puromycin. Plasmid vectors were kindly obtained from K. Cimprich (Stanford University, Stanford, CA) (55). All cell lines were routinely tested for mycoplasma (Sigma-Aldrich; MP0035), and cell identity was confirmed with an STR (short tandem repeat) assay at the start and end of the experimental work by BMR Genomics. Cell-culture conditions, cell treatments, and *BRCA2* gene silencing are described in *SI Appendix, Methods*.

Immunofluorescence Microscopy. Slides were visualized at room temperature by using a fluorescence microscope (Eclipse 90i; Nikon) or high-content imaging system (Operetta; PerkinElmer). Cell seeding was performed on a 35-mm dish, 4-well Nunc Lab-Tek II Chamber Slide System (Nalge Nunc; 154526), or 96-well plate (CellCarrier; PerkinElmer) for Operetta massive cell analysis. Plates were coated or not with poly-L-lysine solution (Merck; P4707). After 24 h from seeding, cells were treated with 10 μM PDS, FG, or FA or 15 μM Braco-19 for the indicated time. For high-throughput cell-image analysis, 96-well plates were scanned using the Operetta High-Content Imaging System (Harmony Imaging 4.1; PerkinElmer). After data acquisition, nuclear foci detection and subsequent analyses were performed with Columbus 2.5.0 software (PerkinElmer). For graphical representation of focus distribution, we used box-and-whisker plots using GraphPad Prism 6 software with the following settings: boxes: 25 to 75 percentile range; whiskers: 10 to 90 percentile range; horizontal bars: median number of foci; "+": mean number of foci. Purification and validation of S9.6 and BG4 antibodies are reported in *SI Appendix, Methods*. Detailed protocols of cell fixation and staining for each antibody and cell-image analyses are reported in *SI Appendix, Methods*.

Genome R-Loop Mapping. We used DNA:RNA immunoprecipitation methodologies to immunoprecipitate and isolate DNA:RNA duplexes from genomic DNA preparations by using S9.6 antibody and to map genome-wide R-loop structures, as described previously (18, 27). A detailed DRIP protocol is

reported in *SI Appendix, Methods*. RNA-seq protocols and bioinformatic tools and procedures of genomic R-loop maps are reported in *SI Appendix, Methods*.

Other Methods and Data Availability. Other standard methods [Western blots, cytofluorimetry, MTT (3-(4,5-dimethylthiazol-2-yl)-2,5-diphenyltetrazolium bromide) proliferation assay, quantitative PCR] and primer sequences are reported in *SI Appendix, Methods*. Sequence DRIP reads are available at the Gene Expression Omnibus database (56).

ACKNOWLEDGMENTS. We acknowledge the Toulouse Regional Imaging–Light Imaging Toulouse CBI Platform and Microscopy Core Facility at Medical Faculty, University of Bonn for technical assistance in high-content microscopy. We thank S. Gabor for providing the HB-8730 hybridoma, S. Balasubramanian for the BG4-expressing plasmid, P. Calsou and S. Britton for the mCherry-RNaseH1–expressing cell line, K. Cimprich for the FLAG-RNaseH1–expressing vector, and Barbara Taurisano for technical help. This work was supported by Associazione Italiana per la Ricerca sul Cancro (AIRC) Grant IG-15886 (to G.C.). A.D.M. and M.R. were supported by University of Bologna PhD student fellowships; S.G.M. was supported by a FIRC postdoc fellowship.

1. Hänsel-Hertsch R, Di Antonio M, Balasubramanian S (2017) DNA G-quadruplexes in the human genome: Detection, functions and therapeutic potential. *Nat Rev Mol Cell Biol* 18:279–284.
2. Balasubramanian S, Hurley LH, Neidle S (2011) Targeting G-quadruplexes in gene promoters: A novel anticancer strategy? *Nat Rev Drug Discov* 10:261–275.
3. Cimino-Reale G, Zaffaroni N, Folini M (2016) Emerging role of G-quadruplex DNA as target in anticancer therapy. *Curr Pharm Des* 22:6612–6624.
4. Müller S, et al. (2012) Pyridostatin analogues promote telomere dysfunction and long-term growth inhibition in human cancer cells. *Org Biomol Chem* 10:6537–6546.
5. Rodriguez R, et al. (2012) Small-molecule-induced DNA damage identifies alternative DNA structures in human genes. *Nat Chem Biol* 8:301–310.
6. Zimmer J, et al. (2016) Targeting BRCA1 and BRCA2 deficiencies with G-quadruplex-interacting compounds. *Mol Cell* 61:449–460.
7. Xu H, et al. (2017) CX-5461 is a DNA G-quadruplex stabilizer with selective lethality in BRCA1/2 deficient tumours. *Nat Commun* 8:14432.
8. Ribeyre C, et al. (2009) The yeast Pif1 helicase prevents genomic instability caused by G-quadruplex-forming CEB1 sequences in vivo. *PLoS Genet* 5:e1000475.
9. Vannier J-BB, Pavicic-Kaltenbrunner V, Petalcorin MIR, Ding H, Boulton SJ (2012) RTEL1 dismantles T loops and counteracts telomeric G4-DNA to maintain telomere integrity. *Cell* 149:795–806.
10. van Wietmarschen N, et al. (2018) BLM helicase suppresses recombination at G-quadruplex motifs in transcribed genes. *Nat Commun* 9:271.
11. Santos-Pereira JM, Aguilera A (2015) R loops: New modulators of genome dynamics and function. *Nat Rev Genet* 16:583–597.
12. Sollier J, Cimprich KA (2015) Breaking bad: R-loops and genome integrity. *Trends Cell Biol* 25:514–522.
13. Skourti-Stathaki K, Proudfoot NJ (2014) A double-edged sword: R loops as threats to genome integrity and powerful regulators of gene expression. *Genes Dev* 28:1384–1396.
14. Chédin F (2016) Nascent connections: R-loops and chromatin patterning. *Trends Genet* 32:828–838.
15. Duquette ML, Handa P, Vincent JA, Taylor AF, Maizels N (2004) Intracellular transcription of G-rich DNAs induces formation of G-loops, novel structures containing G4 DNA. *Genes Dev* 18:1618–1629.
16. Brooks TA, Hurley LH (2009) The role of supercoiling in transcriptional control of MYC and its importance in molecular therapeutics. *Nat Rev Cancer* 9:849–861.
17. Kouzine F, et al. (2013) Transcription-dependent dynamic supercoiling is a short-range genomic force. *Nat Struct Mol Biol* 20:396–403.
18. Ginno PA, Lim YW, Lott PL, Korf I, Chédin F (2013) GC skew at the 5′ and 3′ ends of human genes links R-loop formation to epigenetic regulation and transcription termination. *Genome Res* 23:1590–1600.
19. Aguilera A, Gómez-González B (2017) DNA-RNA hybrids: The risks of DNA breakage during transcription. *Nat Struct Mol Biol* 24:439–443.
20. Sparapani S, et al. (2010) Bis-guanylhydrazone diimidazo[1,2-a:1,2-c]pyrimidine as a novel and specific G-quadruplex binding motif. *Chem Commun (Camb)* 46:5680–5682.
21. Amato J, et al. (2016) Toward the development of specific G-quadruplex binders: Synthesis, biophysical, and biological studies of new hydrazone derivatives. *J Med Chem* 59:5706–5720.
22. Marinello J, Chillemi G, Bueno S, Manzo SG, Capranico G (2013) Antisense transcripts enhanced by camptothecin at divergent CpG-island promoters associated with bursts of topoisomerase I-DNA cleavage complex and R-loop formation. *Nucleic Acids Res* 41:10110–10123.
23. Mouly L, et al. (2018) PARP-1-dependent RND1 transcription induced by topoisomerase I cleavage complexes confers cellular resistance to camptothecin. *Cell Death Dis* 9:931.
24. Sanz LA, et al. (2016) Prevalent, dynamic, and conserved R-loop structures associate with specific epigenomic signatures in mammals. *Mol Cell* 63:167–178.
25. Biffi G, Tannahill D, Miller J, Howat WJ, Balasubramanian S (2014) Elevated levels of G-quadruplex formation in human stomach and liver cancer tissues. *PLoS One* 9:e102711.
26. Chambers VS, et al. (2015) High-throughput sequencing of DNA G-quadruplex structures in the human genome. *Nat Biotechnol* 33:877–881.
27. Manzo SG, et al. (2018) DNA topoisomerase I differentially modulates R-loops across the human genome. *Genome Biol* 19:100.
28. Aguilera A, García-Muse T (2012) R loops: From transcription byproducts to threats to genome stability. *Mol Cell* 46:115–124.
29. Skourti-Stathaki K, Proudfoot NJ, Gromak N (2011) Human senataxin resolves RNA/DNA hybrids formed at transcriptional pause sites to promote Xrn2-dependent termination. *Mol Cell* 42:794–805.
30. Nadel J, et al. (2015) RNA:DNA hybrids in the human genome have distinctive nucleotide characteristics, chromatin composition, and transcriptional relationships. *Epigenetics Chromatin* 8:46.
31. Huppert JL, Balasubramanian S (2007) G-quadruplexes in promoters throughout the human genome. *Nucleic Acids Res* 35:406–413.
32. Britton S, et al. (2014) DNA damage triggers SAF-A and RNA biogenesis factors exclusion from chromatin coupled to R-loops removal. *Nucleic Acids Res* 42:9047–9062.
33. Moynahan ME, Jasin M (2010) Cells have evolved various strategies to contend with the multitude of DNA lesions, including DNA strand breaks, that the genome incurs on a continuous basis. *Nat Rev Mol Cell Biol* 11:196–207.
34. Bell JC, Kowalczykowski SC (2016) Mechanics and single-molecule interrogation of DNA recombination. *Annu Rev Biochem* 85:193–226.
35. Hatch EM, Fischer AH, Deerinck TJ, Hetzer MW (2013) Catastrophic nuclear envelope collapse in cancer cell micronuclei. *Cell* 154:47–60.
36. Yadav P, et al. (2014) Topoisomerase I plays a critical role in suppressing genome instability at a highly transcribed G-quadruplex-forming sequence. *PLoS Genet* 10:e1004839.
37. Mackenzie KJ, et al. (2017) cGAS surveillance of micronuclei links genome instability to innate immunity. *Nature* 548:461–465.
38. Harding SM, et al. (2017) Mitotic progression following DNA damage enables pattern recognition within micronuclei. *Nature* 548:466–470.
39. Bartsch K, et al. (2017) Absence of RNase H2 triggers generation of immunogenic micronuclei removed by autophagy. *Hum Mol Genet* 26:3960–3972.
40. García-Muse T, Aguilera A (2016) Transcription-replication conflicts: How they occur and how they are resolved. *Nat Rev Mol Cell Biol* 17:553–563.
41. Maizels N (2005) Immunoglobulin gene diversification. *Annu Rev Genet* 39:23–46.
42. Hänsel-Hertsch R, et al. (2016) G-quadruplex structures mark human regulatory chromatin. *Nat Genet* 48:1267–1272.
43. Marnef A, Cohen S, Legube G (2017) Transcription-coupled DNA double-strand break repair: Active genes need special care. *J Mol Biol* 429:1277–1288.
44. Clouaire T, Legube G (2015) DNA double strand break repair pathway choice: A chromatin based decision? *Nucleus* 6:107–113.
45. Schiavone D, et al. (2016) PrimPol is required for replicative tolerance of G quadruplexes in vertebrate cells. *Mol Cell* 61:161–169.
46. Yadav P, Owiti N, Kim N (2016) The role of topoisomerase I in suppressing genome instability associated with a highly transcribed guanine-rich sequence is not restricted to preventing RNA:DNA hybrid accumulation. *Nucleic Acids Res* 44:718–729.
47. Lee CG, et al. (2001) Quantitative regulation of class switch recombination by switch region transcription. *J Exp Med* 194:365–374.
48. Barber GN (2015) STING: Infection, inflammation and cancer. *Nat Rev Immunol* 15:760–770.
49. Mouw KW, Goldberg MS, Konstantinopoulos PA, D'Andrea AD (2017) DNA damage and repair biomarkers of immunotherapy response. *Cancer Discov* 7:675–693.
50. Mackenzie KJ, et al. (2016) Ribonuclease H2 mutations induce a cGAS/STING-dependent innate immune response. *EMBO J* 35:831–844.
51. Hiller B, et al. (2012) Mammalian RNase H2 removes ribonucleotides from DNA to maintain genome integrity. *J Exp Med* 209:1419–1426.
52. Sparks JL, et al. (2012) RNase H2-initiated ribonucleotide excision repair. *Mol Cell* 47:980–986.
53. Andreani A, et al. (2004) Potential antitumor agents. 34.(1) Synthesis and antitumor activity of guanylhydrazones from imidazo[2,1-b]thiazoles and from diimidazo[1,2-a:1,2-c] pyrimidine. *Anticancer Res* 24:203–211.
54. Jeanblanc M, et al. (2012) Parallel pathways in RAF-induced senescence and conditions for its reversion. *Oncogene* 31:3072–3085.
55. Stork CT, et al. (2016) Co-transcriptional R-loops are the main cause of estrogen-induced DNA damage. *eLife* 5:e17548.
56. Russo M, et al. (2018) R-loop maps in U2OS cells after G-quadruplex ligands treatment. Gene Expression Omnibus. Available at https://www.ncbi.nlm.nih.gov/geo/query/acc.cgi?acc=GSE115957. Deposited June 18, 2018.